Section-illumination photoacoustic microscopy for dynamic 3D imaging of microcirculation *in vivo*

Liang Song, Konstantin Maslov, and Lihong V. Wang*

Optical Imaging Laboratory, Department of Biomedical Engineering, Washington University in St. Louis, St. Louis, Missouri 63130 USA

**Corresponding author: lhwang@biomed.wustl.edu*

Received February 17, 2010; accepted March 18, 2010;
posted March 31, 2010 (Doc. ID 124273); published April 30, 2010

We developed section-illumination photoacoustic microscopy capable of dynamic *in vivo* imaging of microvessels as small as 30 μm in diameter. The section illumination improved the elevational resolution while an ultrasound array provided the in-plane axial and lateral resolutions. Using the imaging system, we monitored the wash-in dynamics of Evans Blue in the microcirculation of mouse ears at 249 Hz 2D and 0.5 Hz 3D image acquisition rates. Such observation allowed us to differentiate the arterioles from the venules. In the future, the technology may be used to study angiogenesis, diabetes-induced vascular complications, and pharmacokinetics.

OCIS codes: 170.0110, 170.0180, 170.3880, 170.5120.

The microcirculation of blood plays a crucial role in the regulation of hemodynamics and metabolism; its physiological state can indicate many diseases, including diabetes, hypertension, and coronary heart disease. Hence, the study of microcirculation is vital to both clinical practice—e.g., the evaluation of tissue perfusion in the presence of vascular diseases—and preclinical studies—e.g., the assessment of therapeutic efficacy in drug development [1–3]. Many complementary imaging techniques, including nailfold capillaroscopy, polarization spectral imaging, high-frequency ultrasound imaging, and magnetic resonance imaging, have been used to study microcirculation [3–6]. Yet none of them simultaneously offer the desired sensitivity, resolution, and imaging depth in a single modality.

Recently, optical-resolution photoacoustic microscopy (OR-PAM) has emerged as a viable tool for *in vivo* microvascular imaging [7]. OR-PAM provides high optical absorption contrast—from either intrinsic or exogenous absorbers—and axial ultrasonic resolution at depths up to the optical transport mean free path (~1 mm in the skin) [8]. If a single-element ultrasonic transducer is used, the imaging speed is limited by the 2D mechanical scanning for 3D imaging. One solution to improving the speed is to use an ultrasound array. Previously, an ultrasound array was used to accelerate the imaging rate of acoustic-resolution photoacoustic microscopy by ~100-fold from the single-element implementation, reaching a B-scan imaging rate of 166 Hz, a 3D imaging rate of ~0.1 Hz, and a single 3D imaging time of only 1–2 s [9,10]. However, the poor acoustic elevational focus (>200 μm), common to all linear ultrasound arrays, became a bottleneck for spatial resolution [11,12], which limited its application in microcirculation studies (most microvessels have diameters less than 100 μm).

In this work, we developed section-illumination photoacoustic microscopy (SI-PAM) to improve the elevational resolution. Moreover, by optimizing data acquisition and transfer, we improved the imaging speed to 249 Hz for B scans and to 0.5 Hz for continuous 3D scans. SI-PAM was used to image *in vivo* microcirculation dynamics in mouse ears noninvasively. To our knowledge, this is the first report of dynamic 3D *in vivo* photoacoustic imaging with both high temporal and spatial resolutions.

The principles of SI-PAM are shown in Fig. 1. In order to achieve section illumination, the laser beam was first expanded, and then cylindrically focused into the sample. The numerical aperture of the focus was 0.015, which in theory would result in an elevational resolution of 24 μm—tenfold better than the one defined acoustically; the depth of focus in air was ~2.7 mm, greater than the targeted 1 mm imaging depth. To detect the photoacoustic waves from the sample, a custom-built ultrasound array of 30 MHz center frequency was used [9], positioned opposite the laser illumination. Photoacoustically exciting the entire B-scan imaging region with each laser pulse, the section illumination was able to take full advantage of the ultrasound array for high-speed imaging. While 2D B-scan imaging required no mechanical scanning, 3D imaging necessitated linearly translating the sample in the elevational (y) direction. By storing photoacoustic signals in the data acquisition card, we achieved 3D image acquisition at 0.5 Hz, corresponding to a 2D (B-scan) image acquisition rate of 249 Hz. Currently, in order to stream data from the 48-channel ultrasound array to the 8-channel

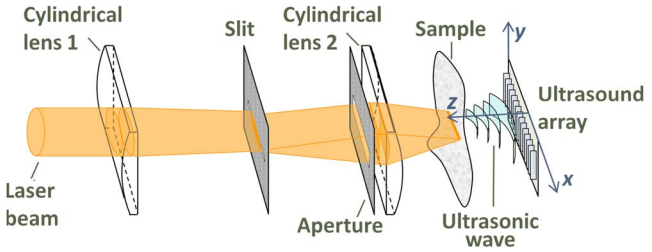

Fig. 1. (Color online) Schematic of the section-illumination photoacoustic microscopy (SI-PAM) system. The widths of the slit and the aperture along the y axis are 50 μm and 5 mm, respectively. Coordinates x, y, and z represent the lateral, elevational, and axial (depth) directions of the ultrasound array, respectively.

data acquisition card, 6 laser pulses were needed for one B-scan. Thus the laser repetition rate corresponding to the 249 Hz B-scan rate was ~1.5 kHz, approximately the highest rate at which our laser could operate. Further details about image acquisition and reconstruction were presented in our previous publications [9,10].

Figures 2(a)–2(c) show that the elevational resolution (y) was improved approximately tenfold, from 200–400 μm to 28 μm, by the section illumination, while the in-plane lateral (x) resolution (~70 μm) was unaffected. Figure 2(d) shows that SI-PAM can penetrate ~1.6 mm through biological tissue. Figure 2(e) is an *in vivo* photoacoustic image of a mouse ear microvasculature acquired by SI-PAM at 584 nm, sensing the intrinsic absorption contrast of hemoglobin. The image is shown in the form of maximum amplitude projection (MAP)—the maximum photoacoustic amplitudes projected along a direction to its orthogonal plane—along the z axis with depth encoded by color. Unless otherwise mentioned, all MAPs are along the z axis. Microvessels in diameters down to 30 μm were clearly imaged, and a predominantly two-layered structure of blood vessels was observed, consistent with the previous results from OR-PAM [13]. Figure 2(f) is a snapshot of a 3D animation (Media 1) showing the mouse ear microvasculature from various perspectives. All animal experiments were carried out, in compliance with Washington University approved protocols.

The dynamic 3D *in vivo* imaging capability of SI-PAM was demonstrated by real-time monitoring of the wash-in dynamics of Evans Blue (EB) dye in mouse ear microcirculation. Swiss Webster mice (Harlan, Inc., USA) weighing ~25 g were used. On injection of ~0.05 ml of 3% EB through the tail vein, the mouse ear was continuously imaged by SI-PAM at 600 nm for up to 2 min at 5 s intervals. At this wavelength, EB has much stronger absorption

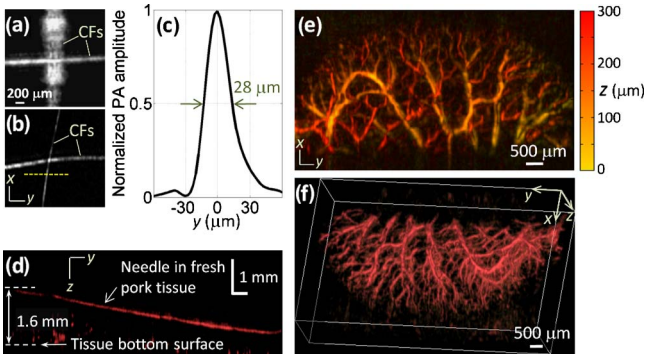

Fig. 2. (Color online) (a), (b) MAP images of two crossed 6 μm diameter carbon fibers (CFs) acquired by PAM at 584 nm without and with section illumination, respectively. (c) Distribution of photoacoustic (PA) amplitude from the vertical carbon fiber along the dashed line in (b). (d) MAP (along the x axis) image of a 250 μm diameter black needle inserted in a fresh pork specimen acquired by SI-PAM at 584 nm. (e) MAP image of a mouse ear microvasculature acquired by SI-PAM noninvasively *in vivo* (at 584 nm). Depth (z)—300 μm in total—is encoded by color. (f) Snapshot of a 3D animation (Media 1) showing the microvasculature in (e).

(which peaks at 620 nm) than hemoglobin, and thus its signal dominates the contrast. Media 2 shows the entire EB wash-in process recorded by SI-PAM, with representative frames shown in Fig. 3. It is clearly seen that the dye progressively reaches different levels of vessel branches—from the root to the edge of the ear—at different time points. Yet the overall wash-in process is as short as 15–20 s. After 1–2 min, the photoacoustic signal decreases [Figs. 3(g) and 3(h)], indicating the beginning of the wash-out of EB. However, the entire wash-out process, which was not monitored in this study, could take up to a few days.

Although the spatial resolution of the SI-PAM was insufficient to resolve closely located arteriole-venule pairs even if the oxygen saturation of hemoglobin were measured spectrally, we found that the dynamics enabled us to distinguish arterioles from venules in the microcirculation. In fact, four distinct stages of the wash-in process can be observed in Media 2 (or Fig. 3):

1. EB dye flowed to the major arterioles at the root of the ear;
2. EB dye reached the arteriole branches and the capillary bed at the edge of the ear;
3. EB dye returned to the venule branches from the capillary bed;
4. EB dye returned to the major venules at the root of the ear.

In the end, the entire microcirculation of the mouse ear was perfused with EB dye. Figure 4 is a pseudocolored composite image showing the separated arterioles (red) and venules (green). Furthermore, Media 3 shows the wash-in dynamics of EB in both gray scale and pseudocolor.

With a 50 Hz B-scan imaging rate, the entire EB uptake process was quantitatively imaged by

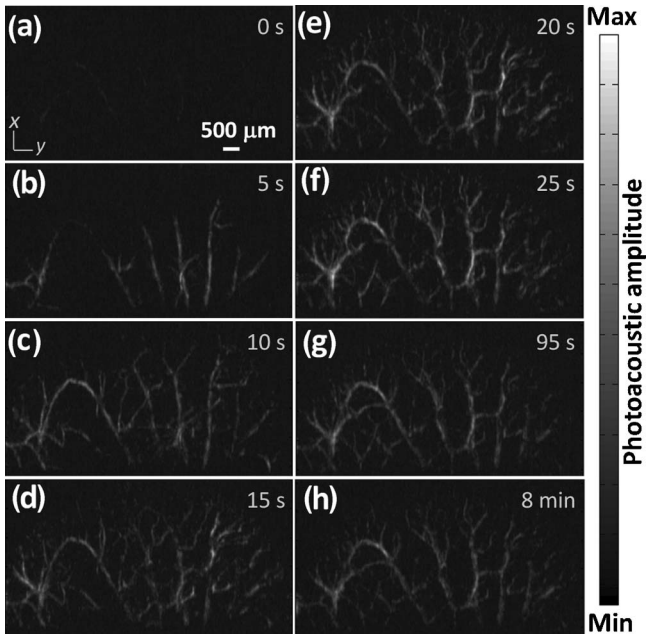

Fig. 3. Wash-in dynamics of EB in a mouse ear microvasculature imaged by SI-PAM at 600 nm (Media 2). (a)–(h) MAP images at representative time points after EB injection.

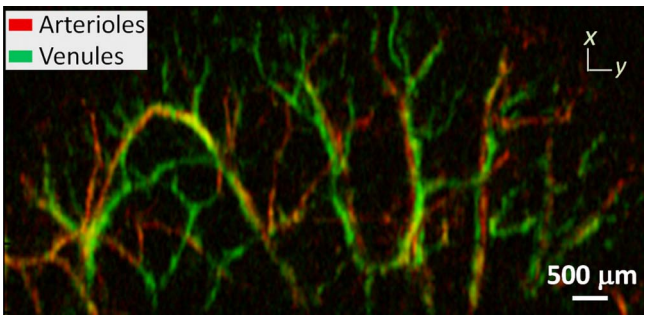

Fig. 4. (Color online) Pseudocolored composite image showing arterioles and venules separated according to the wash-in dynamics of EB (Media 3).

SI-PAM. An MAP image and a representative B-scan image of the mouse ear microvasculature are shown in Figs. 5(a) and 5(b), respectively. Media 4 is a real-time B-scan movie showing the EB uptake in a single vessel (vessel 1). The photoacoustic amplitude representing the dye concentration was quantified as a function of time [Fig. 5(d)]. The EB injection started at $t=0$ s and took ~2 s to complete. At ~14 s, the photoacoustic signal stabilized, suggesting that the dye concentration had reached a steady state in the blood circulation. This stabilization time agreed well with the circulation time needed to fully mix the dye in blood, which was ~15 s as estimated by using a stroke volume of 20 μl, a heartbeat rate of 400 beats/min (mice under anesthesia), and a total blood volume of 2 ml.

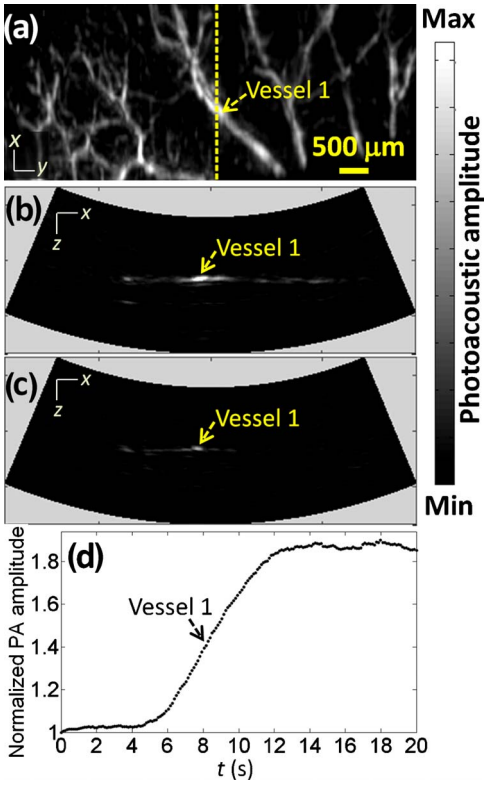

Fig. 5. (Color online) Real-time B-scan imaging of the EB wash-in dynamics in a mouse ear microvasculature. (a) Control MAP image at 584 nm. (b) Control B-scan image at 584 nm corresponding to the dotted line in (a). (c) Snapshot of a B-scan movie (Media 4) of the EB wash-in dynamics acquired at 600 nm. (d) Plot of the EB wash-in dynamics in vessel 1.

In summary, we developed section-illumination photoacoustic microscopy (SI-PAM) that overcomes the poor elevational resolution bottleneck of ultrasound array photoacoustic microscopy: The system offers 28 μm elevational, 25 μm axial, and 70 μm lateral resolutions. In addition, SI-PAM is capable of B-scan and 3D image acquisition at 249 and 0.5 Hz, respectively. The combined high spatial and temporal resolutions permit dynamic 3D imaging of microcirculation *in vivo*. Using SI-PAM, the wash-in dynamics of EB in mouse ear microcirculation were noninvasively imaged and quantified. Major arterioles and venules were differentiated by using the EB wash-in dynamics. In the future, to allow the imaging of more anatomical sites *in vivo*, reflection-mode SI-PAM will be constructed. With this successful demonstration of dynamic 3D *in vivo* imaging of microcirculation, we believe that SI-PAM will open up many new possibilities for the study of angiogenesis, diabetes-induced vascular complications, and pharmacokinetics.

This work was sponsored in part by NIH grants R01 EB000712, EB000712A2S1, R01 EB00071207S2, R01 EB008085, R01 CA113453901, U54 CA136398, and 5P60 DK02057933. L. Wang has a financial interest in Microphotoacoustics, Inc. and Endra, Inc., which, however, did not support this work. The authors thank Chulhong Kim, Song Hu, Junjie Yao, and Changhui Li for beneficial discussions and thank Professor James Ballard for close reading of the manuscript.

References

1. M. J. Leahya, J. G. Enfielda, N. T. Clancya, J. O'Dohertya, P. McNamaraa, and G. E. Nilsson, Med. Laser Appl. **22**, 105 (2007).
2. M. D. Stern, Nature **254**, 56 (1975).
3. W. Groner, J. W. Winkelman, A. G. Harris, C. Ince, G. J. Bouma, K. Messmer, and R. G. Nadeau, Nat. Med. **5**, 1209 (1999).
4. A. F. DeVries, J. Griebel, C. Kremser, W. Judmaier, T. Gneiting, A. Kreczy, D. Ofner, K. P. Pfeiffer, G. Brix, and P. Lukas, Cancer Res. **61**, 2513 (2001).
5. M. Cutolo, A. Sulli, C. Pizzorni, and S. Accardo, J. Rheumatol. **27**, 155 (2000).
6. D. E. Goertz, J. L. Yu, R. S. Kerbel, P. N. Burns, and F. S. Foster, Ultrasound Med. Biol. **29**, 39 (2003).
7. K. Maslov, H. F. Zhang, S. Hu, and L. V. Wang, Opt. Lett. **33**, 929 (2008).
8. L. V. Wang, Nat. Photonics **3**, 503 (2009).
9. L. Song, K. Maslov, R. Bitton, K. K. Shung, and L. V. Wang, J. Biomed. Opt. **13**, 054028 (2008).
10. R. J. Zemp, L. Song, R. Bitton, K. K. Shung, and L. V. Wang, Opt. Express **16**, 7915 (2008).
11. L. Song, K. Maslov, K. K. Shung, and L. V. Wang, J. Biomed. Opt. **15**, 021303 (2010).
12. L. Song, C. Kim, K. Maslov, K. K. Shung, and L. V. Wang, Med. Phys. **36**, 3724 (2009).
13. S. Hu, K. Maslov, and L. V. Wang, Opt. Express **17**, 7688 (2009).